Assessment of velocity-acceleration feedback in optimal control of smart piezoelectric beams

S.B. Beheshti-Aval* and M. Lezgy-Nazargah

Department of Civil Engineering, Khajeh Nasir Toosi University of Technology (KNTU), Tehran, Iran

Abstract. Most of studies on control of beams containing piezoelectric sensors and actuators have been based on linear quadratic regulator (LQR) with state feedback or output feedback law. The aim of this study is to develop velocity-acceleration feedback law in the optimal control of smart piezoelectric beams. A new controller which is an optimal control system with velocity-acceleration feedback is presented. In finite element modeling of the beam, the variation of mechanical displacement through the thickness is modeled by a sinus model that ensures inter-laminar continuity of shear stress at the layer interfaces as well as the boundary conditions on the upper and lower surfaces of the beam. In addition to mechanical degrees of freedom, one electric potential degree of freedom is considered for each piezoelectric element layer. The efficiency of this control strategy is evaluated by applying to an aluminum cantilever beam under different loading conditions. Numerical simulations show that this new control scheme is almost as efficient as an optimal control system with state feedback. However, inclusion of the acceleration in the control algorithm increases practical value of a system due to easier and more accurate measurement of accelerations.

Keywords: active structural control; smart piezoelectric beam; velocity-acceleration feedback.

1. Introduction

Future tendency of engineering researches is toward the structures that are able to sense, respond and minimize the effects of applied disturbance to them. This class of structures is generally called smart structures. In order to achieve the optimal design of structures with required performance, the reduction of vibrations under vibratory loadings is unavoidable. Traditionally passive control is utilized in many structures in order to reduce vibrations. By using passive control in a structure, we are not able to change its damping. In active control strategy, we are able to change the damping of a structure to the required value. By taking the continuing price reduction of electronic components and devices into account, active control was economically compared to passive control. By developing smart structures, piezoelectric material was used as sensors and actuators in order to self-response of structures. Because of small dimensions and light weight, we can use many piezoelectric patches as sensors and actuators, without causing changes in the mass, stiffness and other dynamic properties of the main structure. A review about the static and dynamic control of structures using piezoelectric materials was done by Irschik (2002) and Sunar and Rao (1999).

Piezoelectricity is an electromechanical phenomenon that is produced in some special crystals, and

---

*Corresponding Author, Professor, E-mail: beheshti@kntu.ac.ir

relates displacement and electrical fields to each other. In active control of vibrations, two classes of piezoelectric materials are used widely: piezoceramics and piezopolymers. The piezoceramics do not need the high voltage to act as actuators; therefore they are used widely as both sensors and actuators. In contrast to the piezoceramics, the piezopolymers need the high voltage to act as actuators and therefore are mostly used as sensors (Vasques and Rodrigues 2006).

Various mathematical models have been developed to describe the behavior of structures containing piezoelectric sensors and actuators. These models can be classified into two broad categories as induced strain and coupled electromechanical models. The induced strain models use approximate theories to incorporate the piezoelectric effects. Because the electric potential is not considered as a state variable in the formulation, these models are generally limited in predicting only the active response of piezoelectric materials (Crawley and de Luis 1987, Tzou and Gadre 1989, Wang and Rogers 1991, Sung *et al.* 1996). The coupled electromechanical models are able to predict both the sensor and actuator behavior of piezoelectric materials, due to incorporating both displacements and electric potential as state variables in the formulation (Allik and Hughes 1970, Xu *et al.* 1995, Heyliger *et al.* 1994, Saravanos *et al.* 1997, Lage *et al.* 2004a, 2004b). A survey about formulations and finite element modeling of adaptive piezoelectric structures was done by Benjeddou (2000).

The selection of a control technique is important in designing of controllers. Various strategies have been proposed for the control of structures by piezoelectric materials: passive control which is obtained by connecting electrodes of actuators to a passive electrical network, active control which is obtained by exerting the external voltage to electrodes of piezoactuators, and finally hybrid control which consists of an active control scheme with a passive device. These methods of control were investigated in the following references: Qiu and Tani (1995), Veley and Rao (1996), Lim *et al.* (1997), Oshima *et al.* (1997), Chandrashekhara and Smyser (1998), Blanguernon *et al.* (1999) and Bruant *et al.* (2001).

Active control of structures by piezoelectric materials has been regarded by many researchers and various control algorithms has been proposed to obtain the optimal design and the suitable performance of these structures. A state of the art study about the active vibration control with piezoelectric materials was performed by Benjeddou (2004). Different algorithms used in the active vibration literature can be classified into two categories: feedback control and feedforward control. There is a difference between these two algorithms and each one has its own advantages and limitations. In systems which the excitation of the structure can be directly observed and used as a feedforward control signal, using feedforward control is effective. On the contrary, in systems which the direct measurement of the excitation is not possible, the control signal obtained from the piezoelectric sensors is fed back to the actuators (Alkhatib and Golnaraghi 2003).

This study is focused on feedback control. Most of previous studies on optimal control of smart piezoelectric beams have been based on state feedback or output feedback law. Since the measurement of acceleration is easier and more accurate, addition of the acceleration feedback to the control strategy improves its practical value for applications. In this study, optimal control of piezoactuated beams with velocity-acceleration feedback is evaluated. A new controller which is an optimal control system with velocity-acceleration feedback is designed. This controller not only guarantees the stability of the system but also minimizes a cost function. This cost function is quadratically dependent on derivative of system's state variables and system's control inputs. In finite element modeling, the mechanical part is based on a sinus model and transverse shear strain is represented using a cosine function. This representation of transverse shear strain satisfies continuity condition of the transverse shear stress as well as the boundary conditions on the upper and lower

surfaces of the beam. Concerning the electrical part, a linear electric field is assumed in the thickness direction. In order to assess velocity-acceleration feedback in optimal control, an aluminum cantilever beam under free vibration, impulse excitation, white noise disturbance, impact rectangular and sinusoidal load is controlled by the proposed strategy. The results are compared with the results obtained from a LQR with state feedback law. All of the results of this study are obtained from a MATLAB program whose algorithm is based on the presented control scheme. The obtained numerical simulations show that this control strategy is as efficient as an optimal control system with state feedback.

2. Mathematical model

2.1 Geometry and coordinate system

In this study, the assumed composite beam is made of *NC* layers of different linearly elastic materials. It has a uniform rectangular cross section of height h, width b and its length is L. Each layer may be piezoelectric (actuator and/or sensor) or non-piezoelectric. In Fig. 1, the laminated beam is shown in the Cartesian Coordinate System (x, y, z).

2.2 Governing and constitutive coupled equations

The constitutive equations of a piezoelectric body in its material-axis system could be expressed as

$$\overline{\sigma}_s = \overline{C}_s \overline{\varepsilon}_s \tag{1}$$

where

$$\overline{\sigma}_s = \{\sigma_1 \ \ \sigma_3 \ \ \sigma_5 \ \ D_1 \ \ D_3\}^T$$

$$\overline{\varepsilon}_s = \{\varepsilon_1 \ \ \varepsilon_3 \ \ \varepsilon_5 \ \ -E_1 \ \ -E_3\}^T$$

$$\overline{C}_s = \begin{bmatrix} C & e \\ e^T & -\chi \end{bmatrix}$$

$$C = \begin{bmatrix} c_{11} & c_{12} & 0 \\ c_{22} & c_{22} & 0 \\ 0 & 0 & c_{33} \end{bmatrix}, \ \ e = \begin{bmatrix} 0 & e_{31} \\ 0 & e_{33} \\ e_{15} & 0 \end{bmatrix}, \ \ \chi = \begin{bmatrix} \chi_{11} & 0 \\ 0 & \chi_{33} \end{bmatrix}$$
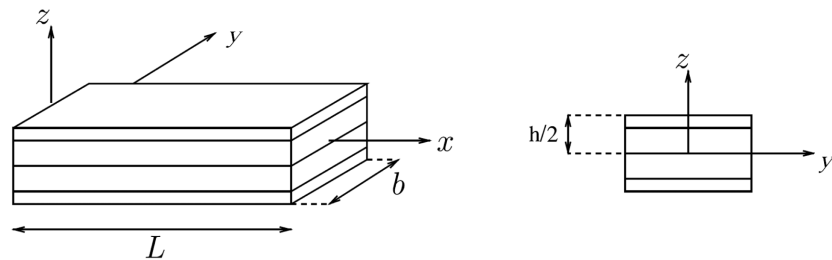

Fig. 1 The laminated beam and co-ordinate system

In the above equations, σ_i and D_i are the components of stress and electric displacement respectively. ε_j and E_j are the components of strain and electric field and c_{ij}, χ_{ij} and e_{ij} are the corresponding elastic, permittivity and piezoelectric constants respectively.

The constitutive equation of a lamina in a common structural axis system could be expressed as

$$\boldsymbol{\sigma} = \boldsymbol{C}_s \boldsymbol{\varepsilon} \tag{2}$$

where

$$\boldsymbol{\sigma} = \{ \sigma_x \quad \sigma_z \quad \tau_{xz} \quad D_x \quad D_z \}^T$$

$$\boldsymbol{\varepsilon} = \{ \varepsilon_x \quad \varepsilon_z \quad \gamma_{xz} \quad -E_x \quad -E_z \}^T$$

$$\boldsymbol{C}_s = \overline{\boldsymbol{T}}^T \overline{\boldsymbol{C}}_s \overline{\boldsymbol{T}} = \begin{bmatrix} \overline{C} & \overline{e} \\ \overline{e}^T & -\overline{\chi} \end{bmatrix}$$

In the above equation, $\overline{\boldsymbol{T}}$ is the transformation matrix. In this study, the non-piezoelectric materials is assumed to be orthotropic and the general type of piezoelectric materials is 'orthorhombic-class $mm2$'.

The principle of virtual work for the piezoelectric medium of volume Ω and regular boundary surface S could be written as (Benjeddou 2000)

$$-\int_\Omega \sigma_{ij} \delta\varepsilon_{ij} \, d\Omega + \int_S F_i \delta u_i \, dS + \int_\Omega f_i \delta u_i \, d\Omega + f_{ci} \delta u_i - \int_\Omega \rho \ddot{u}_i \delta u_i \, d\Omega$$

$$+ \int_\Omega D_i \, \delta E_i \, d\Omega - \int_S \overline{Q} \, \delta\phi \, dS - \int_\Omega \overline{q} \, \delta\phi \, d\Omega = 0 \tag{3}$$

where $F_i, f_i, \overline{q}$ and $\overline{Q}$ are surface force components, mechanical body force components, electrical body charge and surface charge respectively. δu_i and $\delta\phi$ are admissible virtual displacement and potential respectively. ρ is mass density and f_{ci} denotes the components of concentrated loads.

2.3 Displacement and strain fields

The displacement field used in this model is given by (Vidal and Polit 2008)

$$U(x,z,t) = u(x,t) - z\frac{dw(x)}{dx} + (\frac{dw(x)}{dx} + \psi_x(x,t))\{f(z) + \sum_{i=1}^{(NC)-1} \alpha_i(-\frac{1}{2}z + \frac{1}{2}g(z) + (z - z_{i+1})H(z - z_{i+1}))\}$$

$$W(x,z,t) = w(x,t) \tag{4}$$

The functions $U(x, z, t)$ and $W(x, z, t)$ represent the horizontal and vertical displacements respectively. The subfunctions $u(x, t)$ and $w(x, t)$ could be regarded as the mid-plane horizontal and vertical displacements respectively. $\psi_x(x, t)$ is the shear bending rotation around the z axis. H is Heaviside function, and $f(z)$ and $g(z)$ are defined by

$$\begin{cases} f(z) = \dfrac{h}{\pi}\sin(\dfrac{\pi z}{h}) \\ f'(z) = \cos(\dfrac{\pi z}{h}) \end{cases} \qquad \begin{cases} g(z) = \dfrac{h}{\pi}\cos(\dfrac{\pi z}{h}) \\ g'(z) = -\sin(\dfrac{\pi z}{h}) \end{cases}$$

α_i are the continuity coefficients deduced from the physical relations. These continuity coefficients depend on shear modulus of layers. The set of strain equations can be derived using the usual definitions for strain, which becomes

$$\varepsilon_1 = \varepsilon_x = \frac{du}{dx} - z\frac{d^2w}{dx^2} + (\frac{d\psi_x}{dx} + \frac{d^2w}{dx^2})F(z)$$

$$\varepsilon_3 = \varepsilon_z = 0$$

$$\varepsilon_5 = \gamma_{zx} = (\psi_x + \frac{dw}{dx})S(z) \tag{5}$$

where

$$F(z) = f(z) + \sum_{i=1}^{(NC)-1} \alpha_i(-\frac{1}{2}z + \frac{1}{2}g(z) + (z - z_{i+1})H(z - z_{i+1}))$$

$$S(z) = f'(z) + \sum_{i=1}^{(NC)-1} \alpha_i(-\frac{1}{2} + \frac{1}{2}g'(z) + H(z - z_{i+1}) + (z - z_{i+1})\delta(z - z_{i+1}))$$

and $\delta(z-z_{i+1})$ is the first derivative of $H(z-z_{i+1})$.

Using the definitions, the strains $\varepsilon_2 = \varepsilon_4 = \varepsilon_6 = 0$ due to the independence of the *y*-dimension. In preparation for finite element implementation, the displacements and strains, stated by Eqs. (4) and (5) respectively, can be expressed in the following convenient form

$$\boldsymbol{u} = \boldsymbol{A}_u\boldsymbol{u}_u, \quad \varepsilon = \boldsymbol{L}_u\boldsymbol{u}_u \tag{6}$$

where

$$\boldsymbol{u} = \left\{ U \quad W \right\}^T, \, \boldsymbol{u}_u = \left\{ u \quad w \quad \psi_x \right\}^T, \, \varepsilon = \left\{ \varepsilon_1 \quad \varepsilon_3 \quad \varepsilon_5 \right\}^T \text{ and}$$

$$\boldsymbol{A}_u = \begin{bmatrix} 1 & -z\frac{d}{dx} + F(z)\frac{d}{dx} & F(z) \\ 0 & 1 & 0 \end{bmatrix}, \, \boldsymbol{L}_u = \begin{bmatrix} \frac{d}{dx} & -z\frac{d^2}{dx^2} + F(z)\frac{d^2}{dx^2} & F(z)\frac{d}{dx} \\ 0 & 0 & 0 \\ 0 & S(z)\frac{d}{dx} & S(z) \end{bmatrix}$$

2.4 Electric field

Based on successful experiences of Fukunaga *et al.* (2001) and Moita *et al.* (2004), a linear electric potential is assumed along the thickness direction of piezoelectric layers. The electric field vector is the negative gradient of the electric potential, therefore the electric field of *i*-th piezoelectric layer (E_i) could be expressed as

$$\boldsymbol{E}_i = \left\{ \begin{matrix} E_x \\ E_z \end{matrix} \right\}_{layer\,i} = -\nabla\phi_i = -\left\{ \begin{matrix} 0 \\ 1/t_i \end{matrix} \right\}\phi_i \tag{7}$$

where t_i is thickness and ϕ_i is electric potential in *i*-th piezoelectric layer. By introducing the variables $\boldsymbol{B}_\phi^i = \left\{ \begin{matrix} 0 \\ 1/t_i \end{matrix} \right\}$ and $u_\phi^i = \phi_i$, Eq. (7) could be rewritten as
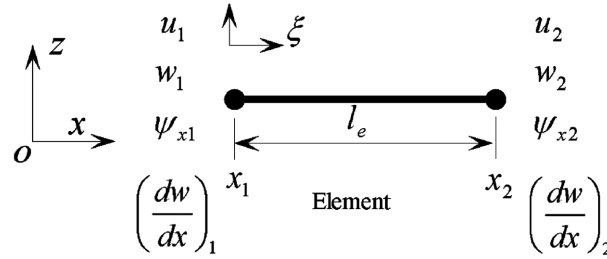
Fig. 2 Two-node beam element

$$E_i = -B_\phi^i u_\phi^i \tag{8}$$

2.5 Finite element modeling

The mechanical element being considered is a *1D* Hermitian beam element for the transverse displacement. This element is shown in Fig. 2. The three mechanical variables $\boldsymbol{u}_u$ could be expressed using four mechanical nodal variables $\boldsymbol{u}_u^e$ as follows

$$\boldsymbol{u}_u = \boldsymbol{N}_u \boldsymbol{u}_u^e \tag{9}$$

Where

$$\boldsymbol{u}_u^e = \{u_1 \quad w_1 \quad \psi_{x1} \quad (dw/dx)_1 \quad u_2 \quad w_2 \quad \psi_{x2} \quad (dw/dx)_2\}^T$$

shape function matrix

$$\boldsymbol{N}_u = \begin{bmatrix} N_1^0 & 0 & 0 & 0 & N_2^0 & 0 & 0 & 0 \\ 0 & N_1 & 0 & N_1'(l_e/2) & 0 & N_2 & 0 & N_2'(l_e/2) \\ 0 & 0 & N_1^0 & 0 & 0 & 0 & N_2^0 & 0 \end{bmatrix}$$

in which N_1^0 and N_2^0 are the Lagrangian shape functions defined as

$$N_1^0 = N_1^0(\xi) = (1-\xi)/2, \quad N_2^0 = N_2^0(\xi) = (1+\xi)/2 \tag{10}$$

and the Hermitian shape functions are

$$N_1 = N_1(\xi) = \frac{1}{4}(1-\xi)^2(2+\xi), \quad N_2 = N_2(\xi) = \frac{1}{4}(2-\xi)(1+\xi)^2$$

$$N_1' = N_1'(\xi) = \frac{1}{4}(1-\xi)^2(1+\xi), \quad N_2' = N_2'(\xi) = -\frac{1}{4}(1-\xi)(1+\xi)^2 \tag{11}$$

where ξ is the local coordinate, defined as

$$\xi = 2\frac{x-x_1}{x_2-x_1} - 1 \tag{12}$$

Using Eqs. (6) and (9), the displacement vector and the strain vector could be expressed as follows

$$\boldsymbol{u} = \boldsymbol{A}_u \boldsymbol{u}_u = \boldsymbol{A}_u \boldsymbol{N}_u \boldsymbol{u}_u^e = \boldsymbol{N} \boldsymbol{u}_u^e$$
$$\varepsilon = \boldsymbol{L}_u \boldsymbol{u}_u = \boldsymbol{L}_u \boldsymbol{N}_u \boldsymbol{u}_u^e = \boldsymbol{B}_u \boldsymbol{u}_u^e$$

(13)

where $\boldsymbol{N}$ and $\boldsymbol{B}_u$ are the displacement and strain interpolation matrices respectively.

In each piezoelectric element layer, the electrical variable u_ϕ could be expressed using one element value u_ϕ^e as follows

$$u_\phi = u_\phi^e$$

(14)

where

$$u_\phi^e = \phi_i$$

Using Eqs. (8) and (14), the electric field $\boldsymbol{E}$ can be expressed as

$$\boldsymbol{E} = -\boldsymbol{B}_\phi \boldsymbol{u}_\phi = -\boldsymbol{B}_\phi \boldsymbol{u}_\phi^e$$

(15)

Substituting Eqs. (2), (13) and (15) into Eq. (3) and assembling the element equations yields the general dynamic equation of the motion

$$\therefore \begin{bmatrix} \boldsymbol{M} & \boldsymbol{0} \\ \boldsymbol{0} & \boldsymbol{0} \end{bmatrix} \begin{bmatrix} \ddot{\boldsymbol{q}}(t) \\ \ddot{\boldsymbol{\varphi}}(t) \end{bmatrix} + \begin{bmatrix} \boldsymbol{K}_{qq} & \boldsymbol{K}_{q\phi} \\ \boldsymbol{K}_{\phi q} & \boldsymbol{K}_{\phi\phi} \end{bmatrix} \begin{bmatrix} \boldsymbol{q}(t) \\ \boldsymbol{\varphi}(t) \end{bmatrix} = \begin{bmatrix} \boldsymbol{F}_q(t) \\ \boldsymbol{F}_\phi(t) \end{bmatrix}$$

(16)

The matrices and vectors in the above equation are the mechanical degrees of freedom $\boldsymbol{q}(t)$, the electrical degrees of freedom $\boldsymbol{\varphi}(t)$, the mass matrix $\boldsymbol{M} = \int_V \rho \boldsymbol{N}^T \boldsymbol{N} \, dV$, the elastic matrix $\boldsymbol{K}_{qq} = \int_V \boldsymbol{B}_u^T \overline{\boldsymbol{C}} \boldsymbol{B}_u \, dV$, the electromechanical coupling matrix $\boldsymbol{K}_{q\phi} = \int_V \boldsymbol{B}_u^T \overline{\boldsymbol{e}} \boldsymbol{B}_\phi \, dV$, the permittivity matrix $\boldsymbol{K}_{\phi\phi} = \int_V \boldsymbol{B}_\phi^T \overline{\boldsymbol{\chi}} \boldsymbol{B}_\phi \, dV$, the mechanical load vector $\boldsymbol{F}_q = \int_V \boldsymbol{N}^T \boldsymbol{f} dV + \int_S \boldsymbol{N}^T \boldsymbol{F} dS + \boldsymbol{N}^T \boldsymbol{f}_c$, and the applied charge vector $\boldsymbol{F}_\phi = \int_S \overline{Q} dS$.

The vector of electric degrees of freedom can be divided into sensors degrees of freedom $\varphi_s(t)$ and actuators degrees of freedom $\varphi_a(t)$. By this division and considering that the external electric charge applied to the sensors is zero, Eq. (16) can be arranged as

$$\begin{bmatrix} \boldsymbol{M}_{qq} & \boldsymbol{0} & \boldsymbol{0} \\ \boldsymbol{0} & \boldsymbol{0} & \boldsymbol{0} \\ \boldsymbol{0} & \boldsymbol{0} & \boldsymbol{0} \end{bmatrix} \begin{bmatrix} \ddot{\boldsymbol{q}}(t) \\ \ddot{\boldsymbol{\varphi}}_a(t) \\ \ddot{\boldsymbol{\varphi}}_s(t) \end{bmatrix} + \begin{bmatrix} \boldsymbol{K}_{qq} & \boldsymbol{K}_{q\phi a} & \boldsymbol{K}_{q\phi s} \\ \boldsymbol{K}_{\phi a q} & \boldsymbol{K}_{\phi a \phi a} & \boldsymbol{K}_{\phi a \phi s} \\ \boldsymbol{K}_{\phi s q} & \boldsymbol{K}_{\phi s \phi a} & \boldsymbol{K}_{\phi s \phi s} \end{bmatrix} \begin{bmatrix} \boldsymbol{q}(t) \\ \boldsymbol{\varphi}_a(t) \\ \boldsymbol{\varphi}_s(t) \end{bmatrix} = \begin{bmatrix} \boldsymbol{F}_q(t) \\ \boldsymbol{F}_{\phi a}(t) \\ \boldsymbol{0} \end{bmatrix}$$

(17)

Without sacrificing accuracy, Eq. (17) can be written as the following form (Moita *et al.* 2004)

$$\boldsymbol{M}_{qq} \ddot{\boldsymbol{q}}(t) + (\boldsymbol{K}_{qq} - \boldsymbol{K}_{q\phi s} \boldsymbol{K}_{\phi s \phi s}^{-1} \boldsymbol{K}_{\phi s q}) \boldsymbol{q}(t) = \boldsymbol{F}_q(t) - \boldsymbol{K}_{q\phi a} \boldsymbol{\varphi}_a(t)$$
$$\boldsymbol{\varphi}_s(t) = -\boldsymbol{K}_{\phi s \phi s}^{-1} \boldsymbol{K}_{\phi s q} \boldsymbol{q}(t)$$

(18)

Since only the lower order modal vibrating are the most significant order in the global response of systems and also the cost of participating of all modal vibrating is relatively high, the mechanical

displacement vector $q(t)$ can be estimated by the modal superposition of the first r modes

$$q(t) = \sum_{i=1}^{r} \boldsymbol{\Psi}_i \eta_i(t) = \hat{\boldsymbol{\Psi}} \boldsymbol{\eta}(t) \tag{19}$$

where $\hat{\boldsymbol{\Psi}} = [\boldsymbol{\Psi}_1, \boldsymbol{\Psi}_2, \ldots, \boldsymbol{\Psi}_r]$ is the truncated modal matrix and $\boldsymbol{\eta}(t) = \{\eta_1(t), \ldots, \eta_r(t)\}^T$ is the corresponding modal coordinates vector. Therefore, system's size is not equal to the number of degrees of freedom obtained from the finite element model. Instead it is equal to the number of modes chosen to model it. According to the orthogonal property of modal vectors with respect to the mass and the stiffness matrix, the damping matrix $\boldsymbol{D}_{qq}$ is chosen such as Narayanan and Balamurugan (2003) and Vasques and Rodrigues (2006)

$$\hat{\boldsymbol{\Psi}}^T \boldsymbol{D}_{qq} \hat{\boldsymbol{\Psi}} = \boldsymbol{\Lambda} \tag{20}$$

where $\boldsymbol{\Lambda}$ is a diagonal modal damping matrix with terms $2\xi_i\omega_i$, ξ_i is the modal damping ratio and ω_i is the natural frequency of i-th mode. According to Eq. (19), by considering the effects of damping, Eq. (18) can be written as

$$\boldsymbol{I}\ddot{\boldsymbol{\eta}}(t) + \boldsymbol{\Lambda}\dot{\boldsymbol{\eta}}(t) + \boldsymbol{\Omega}\boldsymbol{\eta}(t) = -\hat{\boldsymbol{\Psi}}^T \boldsymbol{K}_{\phi aq}^T \boldsymbol{\varphi}_a(t) + \hat{\boldsymbol{\Psi}}^T \boldsymbol{F}_q(t)$$
$$\boldsymbol{\varphi}_s(t) = -\boldsymbol{K}_{\phi s\phi s}^{-1} \boldsymbol{K}_{\phi sq} \hat{\boldsymbol{\Psi}} \boldsymbol{\eta}(t) \tag{21}$$

where $\boldsymbol{I}$ is an identity matrix and $\boldsymbol{\Omega}$ is a diagonal matrix with terms ω_i^2. The generalized eigenvalue problem is solved using the subspace iteration method (Petyt 1990)

3. Active control of vibrations

3.1 State space design

The state space approach is the basis of the modern control and is efficient in systems with several inputs and outputs. In this approach, dynamic systems are described by means of first order differential equations (Kwakernaak and Sivan 1972). Introducing the state space variable $x(t)$ as $x(t) = \{\boldsymbol{\eta}(t), \dot{\boldsymbol{\eta}}(t)\}^T$, Eq. (21) can be written in the following state space form

$$\dot{\boldsymbol{x}}(t) = \boldsymbol{A}\boldsymbol{x}(t) + \boldsymbol{H}_\phi \boldsymbol{f}_\phi(t) + \boldsymbol{H}_q \boldsymbol{f}_q(t)$$
$$\boldsymbol{y}(t) = \begin{cases} \boldsymbol{W}\boldsymbol{x}(t) & \text{\textit{state feedback case}} \\ \boldsymbol{W}\dot{\boldsymbol{x}}(t) & \text{\textit{velocity-acceleration feedback case}} \end{cases} \tag{22}$$

where

$$\boldsymbol{A} = \begin{bmatrix} \boldsymbol{0} & \boldsymbol{I} \\ -\boldsymbol{\Omega} & -\boldsymbol{\Lambda} \end{bmatrix}, \qquad \boldsymbol{H}_q = \begin{bmatrix} \boldsymbol{0} \\ \hat{\boldsymbol{\Psi}}^T \end{bmatrix}, \qquad \boldsymbol{H}_\phi = \begin{bmatrix} \boldsymbol{0} \\ -\hat{\boldsymbol{\Psi}}^T \boldsymbol{K}_{\phi aq}^T \end{bmatrix}$$

$$\boldsymbol{W} = \begin{bmatrix} -\boldsymbol{K}_{\phi s\phi s}^{-1} \boldsymbol{K}_{\phi su} \hat{\boldsymbol{\Psi}} & \boldsymbol{0} \\ \boldsymbol{0} & -\boldsymbol{K}_{\phi s\phi s}^{-1} \boldsymbol{K}_{\phi sq} \hat{\boldsymbol{\Psi}} \end{bmatrix}, \qquad \boldsymbol{f}_q(t) = \boldsymbol{F}_q(t), \qquad \boldsymbol{f}_\phi(t) = \boldsymbol{\varphi}_a(t) \tag{23}$$

$$\boldsymbol{y}(t) = \begin{cases} \{\boldsymbol{\varphi}_s(t), \dot{\boldsymbol{\varphi}}_s(t)\}^T & \text{\textit{state feedback case}} \\ \{\dot{\boldsymbol{\varphi}}_s(t), \ddot{\boldsymbol{\varphi}}_s(t)\}^T & \text{\textit{velocity-acceleration feedback case}} \end{cases}$$

A is called the state space matrix. H_q and H_ϕ are the mechanical and electrical input matrices. W is the output matrix and $y(t)$ is the output vector. $f_q(t)$ and $f_\phi(t)$ are the mechanical and electrical input vectors respectively.

3.2 Optimal control with state feedback

LQR is used in order to determine the control gain. In this case, the gain matrix is designed so that in addition to guarantee the stability of the mechanical system, minimizes a cost function. This cost function is quadratically proportional to system's control inputs and system's state variables

$$J = \int_0^\infty (x^T(t)Qx(t) + f_\phi^T(t)Rf_\phi(t))dt \tag{24}$$

where the weighting matrix Q is a symmetric nonnegative definite matrix which represents the weight attributed to each component of the state variables. In order to account the expenditure of the control signals, the symmetric positive definite weighting matrix R is also used in the cost function. Optimal control with state feedback law can be written as

$$f_\phi(t) = -K_g x(t) = -R^{-1}H_\phi^T Px(t) \tag{25}$$

where K_g is the gain matrix and P is the solution of the following Riccati equation (Kwakernaak and Sivan 1972, Burl 1999)

$$PA + A^T P + Q - PH_\phi R^{-1}H_\phi^T P = 0 \tag{26}$$

Hence, by using the above gain matrix and state feedback law, the closed loop equations of a system can be expressed as

$$\dot{x}(t) = (A - H_\phi K_g)x(t) + H_q f_q(t) \tag{27}$$

3.3 Optimal control with velocity-acceleration feedback

In this section, a velocity-acceleration feedback controller is designed. The gain matrix K_g in the electrical input vector

$$f_\phi(t) = K_g \dot{x}(t) \tag{28}$$

must be determined so that to minimize the following cost function

$$J = \int_0^\infty (\dot{x}^T(t)Q\dot{x}(t) + f_\phi^T(t)Rf_\phi(t))dt \tag{29}$$

where the positive definite (semi-definite) matrix Q is a Hermitian or real symmetric matrix and R is a positive definite Hermitian or real symmetric matrix. By substituting Eq. (28) into Eq. (22), the closed loop equations of a system with velocity-acceleration feedback and without the external disturbance can be written as

$$x(t) = A^{-1}(I - H_\phi K_g)\dot{x}(t) \tag{30}$$

Substituting Eq. (28) into Eq. (29) yields

$$J = \int_0^\infty (\dot{x}^T(t)\,Q\,\dot{x}\,(t) + \dot{x}^T(t)K_g^T\,R\,K_g\,\dot{x}(t)\,)dt \; = \int_0^\infty \dot{x}^T(t)[Q + K_g^T\,R\,K_g]\dot{x}(t)\,dt \tag{31}$$

We assume that the matrix $(A^{-1} - A^{-1}H_\phi K_g)$ is stable. By using the second method of Liapunov, if $(A^{-1} - A^{-1}H_\phi K_g)$ is a stable matrix, there exists a positive definite matrix P which satisfies the following equation

$$P(A^{-1} - A^{-1}H_\phi K_g) + (A^{-1} - A^{-1}H_\phi K_g)^T P = -[Q + K_g^T\,R\,K_g] \tag{32}$$

From Eq. (32), it can be concluded

$$-\dot{x}^T(t)[P(A^{-1} - A^{-1}H_\phi K_g) + (A^{-1} - A^{-1}H_\phi K_g)^T P]\dot{x}(t) = \dot{x}^T(t)[Q + K_g^T\,R\,K_g]\dot{x}(t) \tag{33}$$

By using Eq. (30), Eq. (33) could be rewritten as

$$-\dot{x}^T(t)P\,x(t) - x^T(t)P\,\dot{x}(t) = \dot{x}^T(t)[Q + K_g^T\,R\,K_g]\dot{x}(t)$$

or

$$\dot{x}^T(t)[Q + K_g^T\,R\,K_g]\dot{x}(t) = -\frac{d}{dt}[x^T(t)\,P\,x(t)] \tag{34}$$

Substituting Eq. (34) into Eq. (31) gives

$$J = \int_0^\infty \dot{x}^T(t)[Q + K_g^T\,R\,K_g]\dot{x}(t)\,dt = -x^T(\infty)\,P\,x(\infty) + x^T(0)\,P\,x(0) \tag{35}$$

Since all the eigenvalues $(A^{-1} - A^{-1}K_g H_\phi)$ are assumed to have negative real parts, $x(\infty) \to 0$. Therefore, Eq. (35) reduces to

$$J = x^T(0)Px(0) \tag{36}$$

Since R has been assumed to be a positive definite Hermitian or real symmetric matrix, it can be expressed as

$$R = T^T T \tag{37}$$

where T is a nonsingular matrix. Then Eq. (32) can be written as

$$(I - K_g^T H_\phi^T)(A^{-1})^T P + PA^{-1}(I - H_\phi K_g) + Q + K_g^T T^T T K_g = 0 \tag{38}$$

Rewritten the last equation yields

$$(A^{-1})^T P + PA^{-1} + [T K_g - (T^T)^{-1}H_\phi^T(A^{-1})^T P]^T[T K_g - (T^T)^{-1}H_\phi^T(A^{-1})^T P]$$
$$- PA^{-1}H_\varphi R^{-1}H_\phi^T(A^{-1})^T P + Q = 0 \tag{39}$$

The minimization of J with respect to the elements of K_{ij} of K_g can be accomplished by setting $\partial J/\partial K_{ij} = \partial(x^T(0)Px(0))/\partial K_{ij}$ equal to zero and solving it for the optimal values of K_{ij}. From Eq. (39), the

condition of $\partial(\mathbf{x}^T(0)\mathbf{P}\mathbf{x}(0))/\partial K_{ij} = 0$ (for any given initial conditions $\mathbf{x}(0)$) leads to

$$\mathbf{T}\mathbf{K}_g - (\mathbf{T}^T)^{-1}\mathbf{H}_\phi^T(\mathbf{A}^{-1})^T\mathbf{P} = 0 \tag{40}$$

or

$$\mathbf{T}\mathbf{K}_g = (\mathbf{T}^T)^{-1}\mathbf{H}_\phi^T(\mathbf{A}^{-1})^T\mathbf{P} \tag{41}$$

or

$$\mathbf{K}_g = \mathbf{T}^{-1}(\mathbf{T}^T)^{-1}\mathbf{H}_\phi^T(\mathbf{A}^{-1})^T\mathbf{P} = \mathbf{R}^{-1}\mathbf{H}_\phi^T(\mathbf{A}^{-1})^T\mathbf{P} \tag{42}$$

Eq. (42) yields the optimal gain matrix. By substituting Eq. (42) into Eq. (38), it's easily deduced that $\mathbf{P}$ in Eq. (42) must satisfy the following equation

$$(\mathbf{A}^{-1})^T\mathbf{P} + \mathbf{P}\mathbf{A}^{-1} - \mathbf{P}\mathbf{A}^{-1}\mathbf{H}_\phi\mathbf{R}^{-1}\mathbf{H}_\phi^T(\mathbf{A}^{-1})^T\mathbf{P} + \mathbf{Q} = 0 \tag{43}$$

Therefore, the elements of $\mathbf{P}$ must be determined from Eq. (43) and checked whether $\mathbf{P}$ is positive definite or not. By using the second method of Liapunov, if we solve Eq. (43) and find one positive definite matrix $\mathbf{P}$, the velocity-acceleration feedback system is stable. Finally, the closed loop state equations of a system with velocity-acceleration feedback are given by

$$\dot{\mathbf{x}}(t) = \mathbf{G}^{-1}\mathbf{A}\mathbf{x}(t) + \mathbf{G}^{-1}\mathbf{H}_q\,\mathbf{f}_q(t) \tag{44}$$

where

$$\mathbf{G} = \mathbf{I} - \mathbf{H}_\phi\mathbf{K}_g \tag{45}$$

4. Case studies and discussion

This section aims to assess velocity-acceleration feedback in optimal control of beams containing piezoelectric sensors and actuators. The response of an aluminum cantilever beam under free vibration, white noise disturbance, impulse excitation, impact rectangular and sinusoidal load is evaluated in three conditions: 1) without control, 2) control with state feedback and 3) control with velocity-acceleration feedback. In Fig. 3, this cantilever beam and its piezoelectric sensor and actuator is shown. This beam is 400 mm long, 2 mm thick and 15 mm wide. The piezoelectric sensor and actuator patches are made of PXE-5. Both the piezoelectric sensor and actuator are 40 mm long, 15 mm wide and 1 mm thick, and were located 10 mm from the clamped edge. The mechanical and electrical properties of the aluminum and piezoceramic are shown in Table 1. In finite element
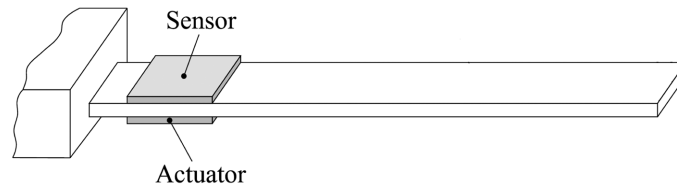

Fig. 3 Smart piezoelectric beam

Table 1 Physical property of aluminum and piezoceramic (data obtained from Vasques and Rodrigues 2006)

Aluminium		PXE-5			
E	70×10^9 Pa	c_{11}^E	131.1×10^9 Pa	d_{31}	-215×10^{-12} mV^{-1}
v	0.3	c_{12}^E	7.984×10^9 Pa	d_{33}	500×10^{-12} mV^{-1}
ρ	2710 kg m^{-3}	c_{13}^E	8.439×10^9 Pa	d_{15}	515×10^{-12} mV^{-1}
G	27.6×10^9 Pa	c_{33}^E	12.31×10^9 Pa	$\varepsilon_{11}^T/\varepsilon_0$	1800
		c_{44}^E	2.564×10^9 Pa	$\varepsilon_{33}^T/\varepsilon_0$	2100
		c_{66}^E	2.564×10^9 Pa	ρ	7800 kg m^{-3}

model, the beam and its piezopatchs are discretized into 48 elements with equal length. In the analysis only first four modal vibrating of the beam are considered. The damping ratio of these first four modes is assumed to be 0.01. Since applying the high voltage to piezoelectric actuators causes reducing or complete vanishing of piezoelectric properties, the elements of the weighing matrices R and Q are chosen so that the control voltage not to exceed 300 V. Based on successful study of Vasques and Rodrigues (2006), the diagonal form $R = diag(I,I)$ and $Q = diag(\Omega, 0)$ are chosen for the weighting matrices.

4.1 White noise disturbance

A white noise disturbance with variance equal to $4 \times 10^{-4} N^2$ is applied to the free end of the beam. The open- and closed-loop tip displacement and sensed voltages, evaluated with both control strategies are shown in Figs. 4(a) and 4(b). For the state feedback case, the weighing matrices $Q = 1\times10^{10} \, diag(\omega_1^2,\omega_1^2,\omega_1^2,\omega_1^2,0,0,0,0)$ and $R = 1 \times I$ were utilized, and for the velocity-acceleration feedback case, the matrices $Q = 1\times10^6 \, diag(\omega_1^2,\omega_1^2,\omega_1^2,\omega_1^2,0,0,0,0)$ and $R = 1.02 \times I$ were chosen. This special choice of the weighing matrices causes that both controllers reduce the magnitude of the maximum vertical displacement by 78%. The actuator and the cumulative actuator voltage with respect to time are shown in Figs. 5(a) and 5(b). The maximum required voltage in the control with state feedback is 128 V. This value in the control with velocity-acceleration feedback is 147 V. These results show that in this case, the control with state feedback has a better performance than the one with velocity-acceleration feedback and requires the lower control voltage.
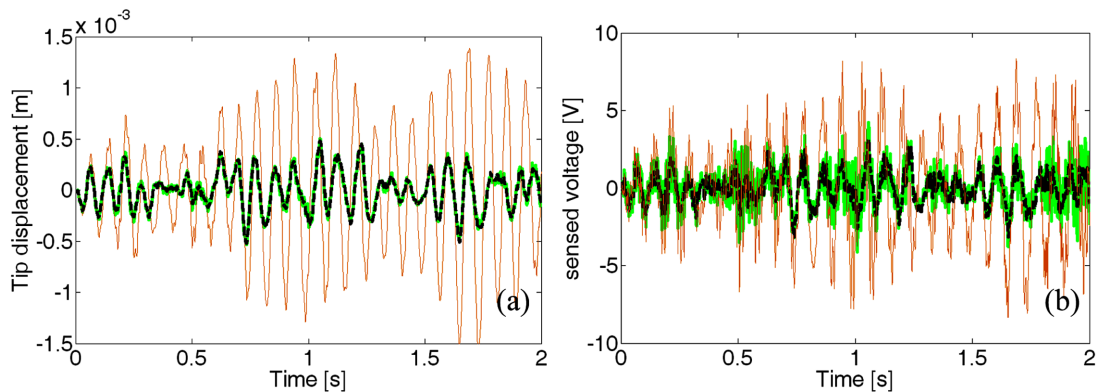

Fig. 4 (a) Tip displacement and (b) sensed voltage for white noise force: — open-loop, — state feedback, ----- velocity-acceleration feedback
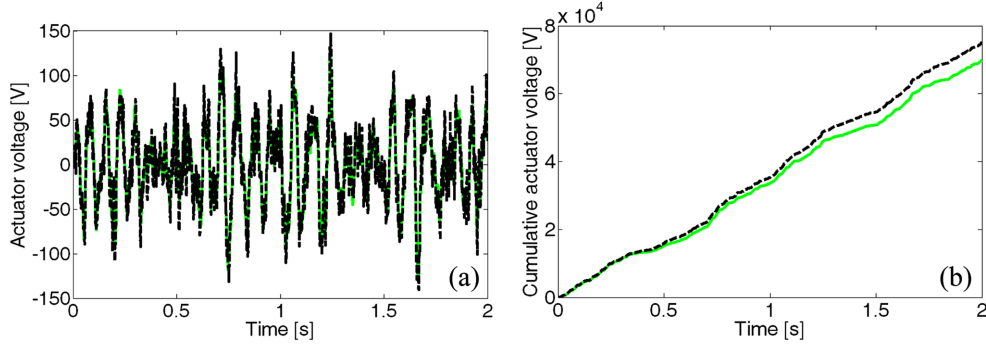
Fig. 5 (a) Actuator voltage and (b) cumulative actuator voltage respect to time for a white noise force: —— state feedback, ----- velocity-acceleration feedback
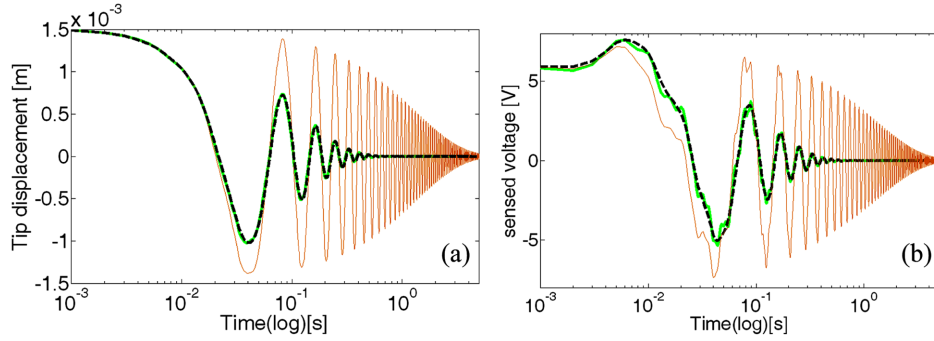

Fig. 6 (a) Tip displacement and (b) sensed voltage for an initial displacement: —— open-loop, —— state feedback, ----- velocity-acceleration feedback

4.2 Initial displacement field

A mechanical load is applied to the free end of the beam so that it produces a vertical displacement equal to 1.5 mm in the tip of the beam. The open- and closed-loop sensed voltages and tip displacement time history for both control strategies are presented in Figs. 6(a) and 6(b). The actuator and the cumulative actuator voltage with respect to time are shown in Figs. 7(a) and 7(b). For the state feedback case, the weighting matrices $Q = 10^{10} \, diag(\omega_1^2, \omega_1^2, \omega_1^2, \omega_1^2, 0,0,0,0)$ and $R = 3 \times I$, were utilized, and for the velocity-acceleration feedback case, the matrices $Q = 10^6 \, diag (\omega_1^2, \omega_1^2, \omega_1^2, \omega_1^2, 0,0,0,0)$ and $R = 1.8 \times I$ were chosen. With this special choice of the weighing matrices, the response of the beam with both control strategies took 1.04s to settle. The maximum required voltage in the control with state feedback is 214 V while this value in the control with velocity-acceleration feedback is 216 V. Considering these results, it can be deduced that in this case, both control strategies have an equal efficiency and also require to the equal control voltage.

4.3 Impact rectangular load

In this case, a rectangular load of $0.05N$ with $0.5s$ duration is assumed to act at the free end of the beam. The open- and closed-loop tip displacement and sensed voltages, evaluated with both controllers
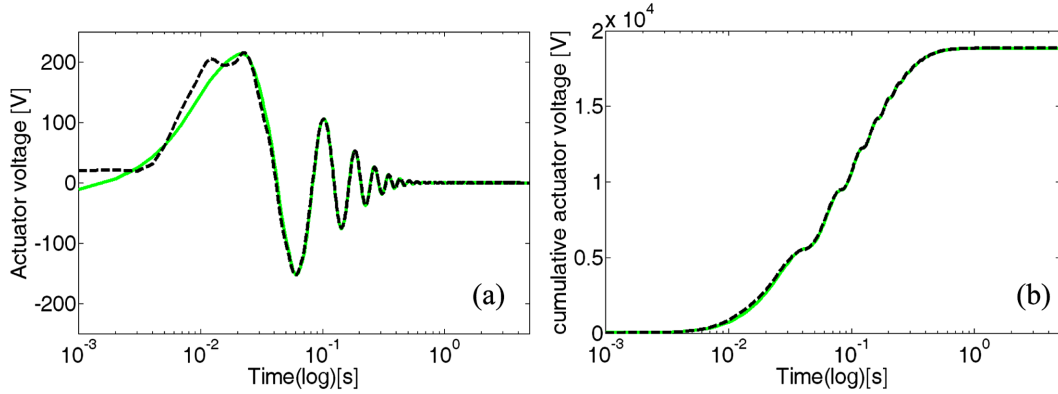
Fig. 7 (a) Actuator voltage and (b) cumulative actuator voltage respect to time for an initial displacement: —— state feedback, ----- velocity-acceleration feedback
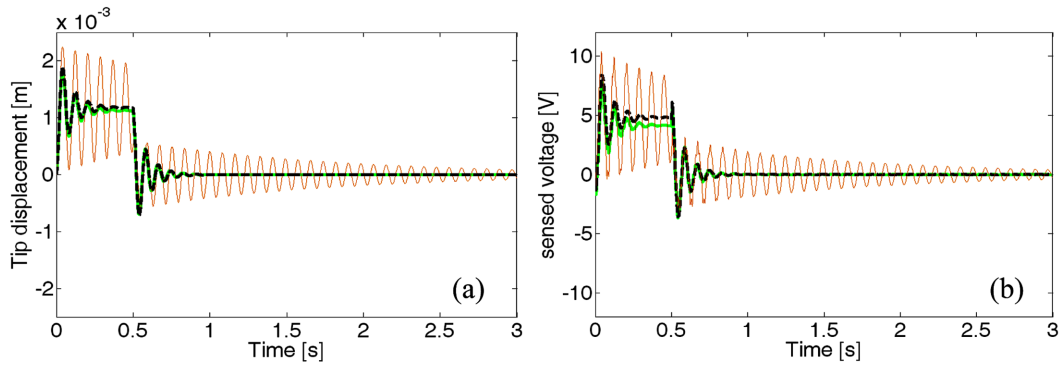

Fig. 8 (a) Tip displacement and (b) sensed voltage for an impact rectangular load: —— open-loop, —— state feedback, ----- velocity-acceleration feedback

are presented in Figs. 8(a) and 8(b). For the state feedback case, the weighing matrices $\boldsymbol{Q} = 10^{10} \, diag$ $(\omega_1^2, \omega_1^2, \omega_1^2, \omega_1^2, 0,0,0,0)$ and $\boldsymbol{R} = 1.75 \times \boldsymbol{I}$, were utilized, and for the velocity-acceleration feedback case, the matrices $\boldsymbol{Q} = 1 \times 10^6 \, diag(\omega_1^2, \omega_1^2, \omega_1^2, \omega_1^2, 0,0,0,0)$ and $\boldsymbol{R} = 1.02 \times \boldsymbol{I}$ were chosen. With this special choice of weighing matrices, the response of beam with both control strategies takes $1.266s$ to settle. In Figs. 9(a) and 9(b), the actuator and cumulative actuator voltage with respect to time are shown. The maximum required voltage in the control with state feedback is 240 V. This value in the control with velocity-acceleration feedback is 214 V. These results show that in this case, the control with velocity-acceleration feedback is more efficient than the control with state feedback, and lower control voltage is required.

4.4 Sinusoidal load

A harmonic load of $0.01\sin(24\pi t)N$ is applied to the tip of the beam. The open- and closed-loop tip displacement and sensed voltages, evaluated with both controllers, are presented in Figs. 10(a) and 10(b). For the state feedback case, the weighing matrices $\boldsymbol{Q} = 10^{10} \, diag$ $(\omega_1^2, \omega_1^2, \omega_1^2, \omega_1^2, 0, 0,0,0)$ and $\boldsymbol{R} = 1.75 \times \boldsymbol{I}$, were utilized, and for the velocity-acceleration feedback case, the matrices
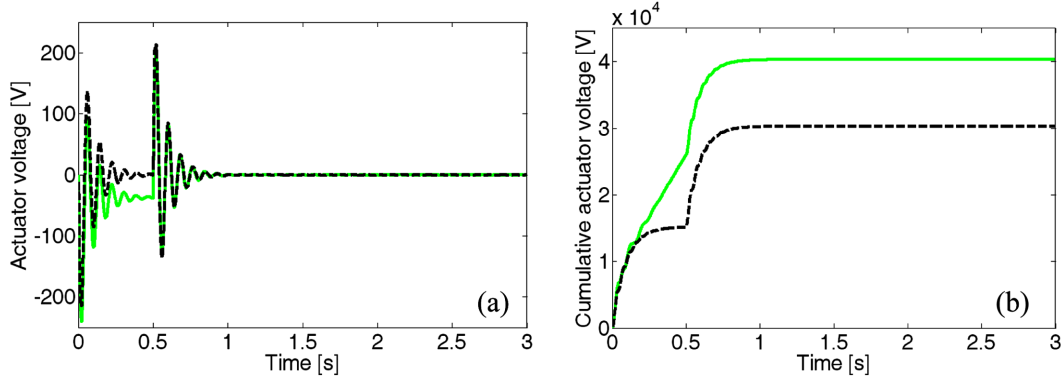
Fig. 9 (a) Actuator voltage and (b) cumulative actuator voltage respect to time for an impact rectangular load: —— state feedback, ----- velocity-acceleration feedback
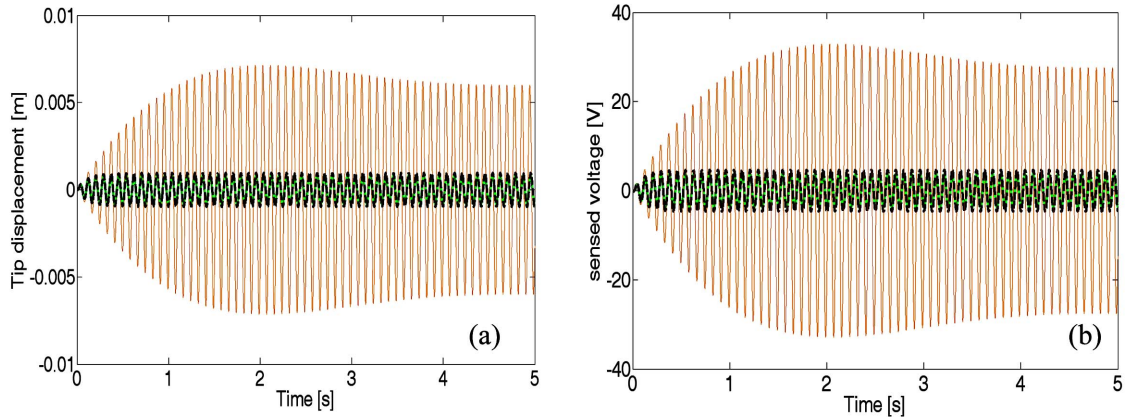

Fig. 10 (a) Tip displacement and (b) sensed voltage for a sinusoidal load: —— open-loop, —— state feedback, ----- velocity-acceleration feedback

$Q = 1\times10^6 \ diag(\omega_1^2, \omega_1^2, \omega_1^2, \omega_1^2, 0, 0, 0, 0)$ and $R = 1.3 \times I$ were chosen. This special choice of the weighing matrices causes that both controllers reduce the magnitude of the maximum vertical displacement by 90%. In Figs. 11(a) and 11(b), the actuator and cumulative actuator voltage with respect to time are presented. The maximum required voltage in the both controllers is 177 V. These results show that in this case, both controllers have an equal efficiency and need to the equal control voltage.

4.5 Impulse excitation

An impulse load of 0.2N, starting at the time $t = 0.5$s is assumed to act at the free end of the beam for 1ms duration. The open- and closed-loop tip displacement and sensed voltages, evaluated with both control strategies are presented in Figs. 12(a) and 12(b). For the state feedback case, the weighing matrices $Q = 10^{10} \ diag(\omega_1^2, \omega_1^2, \omega_1^2, \omega_1^2, 0, 0, 0, 0)$ and $R = 1.75 \times I$, were utilized, and for the velocity-acceleration feedback case, the matrices $Q = 1\times10^6 \ diag(\omega_1^2, \omega_1^2, \omega_1^2, \omega_1^2, 0, 0, 0, 0)$ and $R = 1.1 \times I$ were chosen. With this special choice of weighing matrices, the response of the beam with both

Fig. 11 (a) Actuator voltage and (b) cumulative actuator voltage respect to time for a sinusoidal load: —— state
feedback, ----- velocity-acceleration feedback

Fig. 12 (a) Tip displacement and (b) sensed voltage for an impulse load: —— open-loop, —— state feedback,
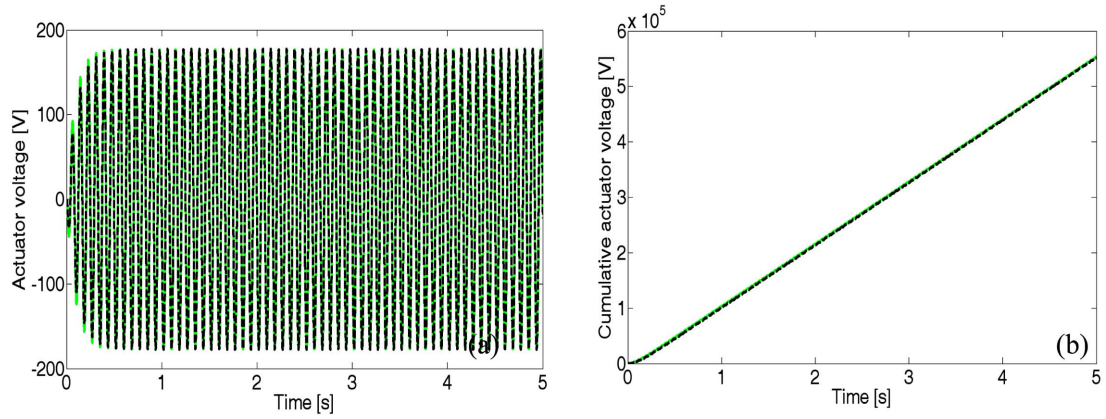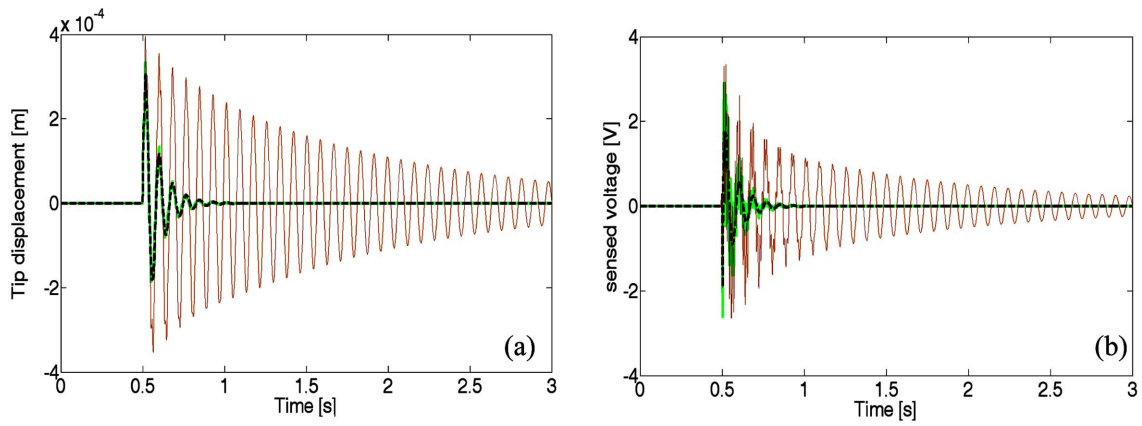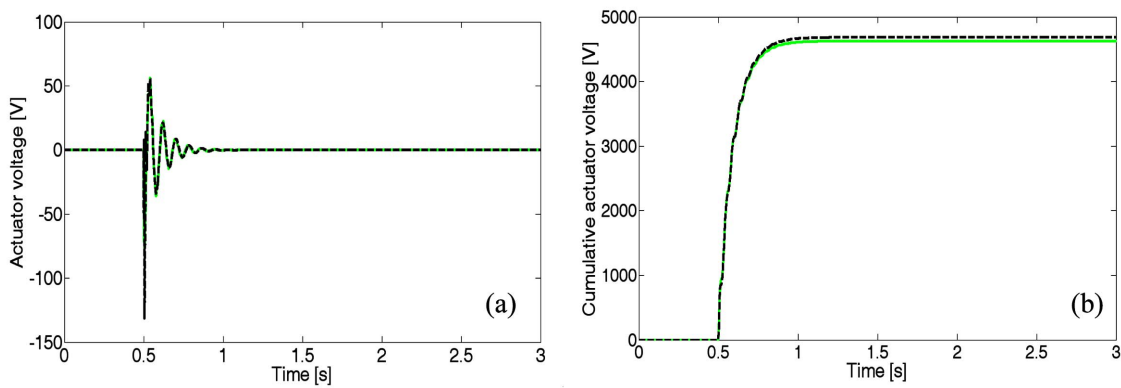----- velocity-acceleration feedback

Fig. 13 (a) Actuator voltage and (b) cumulative actuator voltage respect to time for an impulse load: —— state
feedback, ----- velocity-acceleration feedback

control strategies settles at the time instant $t = 1.19$s. In Figs. 13(a) and 13(b), the actuator and cumulative actuator voltage with respect to time are shown. The maximum required voltage in the control with state feedback is 96 V. In the control with velocity-acceleration feedback this value is 130 V. Although the maximum voltage in the control with velocity-acceleration feedback is higher than one with state feedback, it can be deduced from the cumulative actuator voltage diagram that in this case, both control strategies have almost an equal efficiency.

5. Conclusions

A stable controller for optimal control of smart piezoelectric beams is presented. This controller is an optimal control system with velocity-acceleration feedback law. The optimal stable controller is obtained using the second method of Lyapunov and minimizing a cost function proportional to the derivative of system's state variables and system's control inputs. A two-nodded element is considered in finite element modeling of the beam. It is based on a sinus model for mechanical part. For each element layer of the beam which acts as sensor or actuator, a linear electric field is assumed in the thickness direction. All the interface and boundary conditions are satisfied.

The analyzed case study is an aluminum cantilever beam with a pair of piezoelectric patches. The response of this beam under free vibration, impulse excitation, sinusoidal load, white noise disturbance and impact rectangular load is controlled using the proposed strategy. In order to assess and discuss the efficiency of this new control scheme, the obtained results were compared with the results obtained from LQR with state feedback law. It was shown that for an initial displacement field, both control strategies require almost equal voltage. In control of vibration resulted from a white noise disturbance applied on the tip of the beam, the controller with state feedback requires the lower control voltage and its efficiency is slightly better than the controller with velocity-acceleration feedback. In case of applying impact rectangular load at the free end of the beam, control with velocity-acceleration feedback is most efficient than control with state feedback and requires the lower voltage. In the control of vibration resulted from a sinusoidal and an impulse load applied on the tip of the beam, both control strategies have the same efficiency. Nonetheless, control with velocity-acceleration feedback improves the practical efficiency of a system, due to difficulties in measuring system's displacements. This new feedback control can be used experimentally for future developments.

References

Alkhatib, R. and Golnaraghi, M.F. (2003), "Active structural vibration control: a review", *Shock Vib. Digest*, **35**(5), 367-383.
Allik, H. and Hughes, T.J.R. (1970), "Finite element method for piezoelectric vibration", *Int. J. Num. Meth. Eng.*, **2**(2), 151-157.
Benjeddou, A. (2000), "Advances in piezoelectric finite element modeling of adaptive structural elements: a survey", *Comput. Struct.*, **76**, 347-363.
Benjeddou, A. (2004), *Modeling and simulation of adaptive structures and composites: current trends and future directions, Progress in computational structures technology,* (Eds. Topping, B.H.V. and Soares, C.A.M.), Saxe Coburg Publications.
Blanguernon, A., Léné, F. and Bernadou, M. (1999), "Active control of a beam using a piezoceramic element",

Smart Mater. Struct., **8**(1), 116-124.

Bruant, I., Coffignal, G., Lené, F. and Vergé, M. (2001), "Active control of beam structures with piezoelectric actuators and sensors: modeling and simulation", *Smart Mater. Struct.*, **10**(2), 404-408.

Burl, J.B. (1999), *Linear optimal control*, Addison-Wesley, California.

Chandrashekhara, K. and Smyser, C.P. (1998), "Dynamic modeling and neural control of composite shells using piezoelectric devices", *J. Intel. Mat. Syst. Str.*, **9**(1), 29-43.

Crawley, E.F. and de Luis, J. (1987), "Use of piezoelectric actuators as element of intelligent structures", *AIAA J.*, **25,** 1373-1385.

Fukunaga, H., Hu, N. and Ren, G.X. (2001), "FEM modeling of adaptive composite structures using a reduced higher-order plate theory via penalty functions", *Int. J. Solids Struct.*, **38**, 8735-8752.

Heyliger, P., Ramirez, G. and Saravanos, D. (1994), "Coupled discrete-layer finite elements for laminated piezoelectric plates", *Commun. Numer. Meth. En.*, **10**(12), 971-981.

Irschik, H. (2002), "A review on static and dynamic shape control of structures by piezoelectric actuation", *Eng. Struct.*, **24**, 5-11.

Kwakernaak, H. and Sivan, R. (1972), *Linear optimal control systems*, New York, John Whiley and Sons.

Lage, R.G., Soares, C.M.M., Soares, C.A.M. and Reddy, J.N. (2004a), "Analysis of laminated adaptive plate structures by mixed layerwise finite element models", *Compos. Struct.*, **66**, 269-276.

Lage, R.G., Soares, C.M.M., Soares, C.A.M. and Reddy, J.N. (2004b), "Modeling of piezolaminated plates using layerwise mixed finite element models", *Comput. Struct.*, **82**(23-26), 1849-1863.

Lim, Y.H., Varadan, V.V. and Varadan, V.K. (1997), "Closed loop finite element modeling of active structural damping in the frequency domain", *Smart Mater. Struct.*, **6**(2), 161-168.

Moita, J.M.S., Correia, I.F.P., Soares, C.M.M. and Soares, C.A.M. (2004), "Active control of adaptive laminated structures with bonded piezoelectric sensors and actuators", *Comput. Struct.*, **82**(17-19), 1349-1358.

Narayanan, S. and Balamurugan, V. (2003), "Finite element modelling of piezolaminated smart structures for active vibration control with distributed sensors and actuators", *J. Sound Vib.*, **262**, 529-562.

Oshima, K., Takigami, T. and Hayakawa, Y. (1997), "Robust vibration control of a cantilever beam using selfsensing actuator", *JSME Int. J. C-Mech. Sy.*, **40**, 681-687.

Petyt, M. (1990), *Introduction to finite element vibration analysis*, Cambridge University Press, Cambridge.

Qiu, J. and Tani, J. (1995), "Vibration control of a cylindrical shell using distributed piezoelectric sensors and actuators", *J. Intel. Mat. Syst. Str.*, **6**(4), 474-481.

Saravanos, D.A., Heyliger, P.R. and Hopkins, D.A. (1997), "Layerwise mechanics and finite element model for the dynamic analysis of piezoelectric composite plates", *Int. J. Solids Struct.*, **34**(3), 359-378.

Sunar, M. and Rao, S.S. (1999), "Recent advances in sensing and control of flexible structures via piezoelectric material technology", *Appl. Mech. Rev.*, **52**, 1-16.

Sung, C.K., Chen, T.F. and Chen, S.G. (1996), "Piezoelectric modal sensor actuator design for monitoring generating flexural and torsional vibrations of cylindrical shells", *J. Vib. Acoust.*, **118**, 48-55.

Tzou, H.S. and Gadre, M. (1989), "Theoretical-analysis of a multi-layered thin shell coupled with piezoelectric shell actuators for distributed vibration controls", *J. Sound Vib.*, **132**, 433-450.

Vasques, C.M.A. and Rodrigues, J.D. (2006), "Active vibration control of smart piezoelectric beams: Comparison of classical and optimal feedback control strategies", *Comput. Struct.*, **84**(22-23), 1402-1414.

Veley, D.E. and Rao, S.S. (1996), "A comparison of active, passive and hybrid damping in structural design", *Smart Mater. Struct.*, **5**(5), 660-671.

Vidal, P. and Polit, O. (2008), "A family of sinus finite elements for the analysis of rectangular laminated beams", *Compos. Struct.*, **84**, 56-72.

Wang, B.T. and Rogers, C.A. (1991), "Laminate plate-theory for spatially distributed induced strain actuators", *J. Compos. Mater.*, **25**, 433-452.

Xu, K.M., Noor, A.K. and Tang, Y.Y. (1995), "3-dimensional solutions for coupled thermoelectroelastic response of multilayered plates", *Comput. Method. Appl. M.*, **126**(3-4), 355-371.

CC